TU Delft

Delft University of Technology

Junction temperature and luminous flux prediction for white LED array based on electrical-photo-thermal modeling

Liu, Minne; Li, Wenyu; Chen, Wei; Ibrahim, Mesfin S.; Xiong, Jingkang; Zhang, Guoqi; Fan, Jiajie

DOI
10.1016/j.csite.2023.103940

Publication date
2024

Document Version
Final published version

Published in
Case Studies in Thermal Engineering

Citation (APA)
Liu, M., Li, W., Chen, W., Ibrahim, M. S., Xiong, J., Zhang, G., & Fan, J. (2024). Junction temperature and luminous flux prediction for white LED array based on electrical-photo-thermal modeling. *Case Studies in Thermal Engineering*, *54*, Article 103940. https://doi.org/10.1016/j.csite.2023.103940

Important note
To cite this publication, please use the final published version (if applicable).
Please check the document version above.

Copyright
Other than for strictly personal use, it is not permitted to download, forward or distribute the text or part of it, without the consent of the author(s) and/or copyright holder(s), unless the work is under an open content license such as Creative Commons.

Takedown policy
Please contact us and provide details if you believe this document breaches copyrights.
We will remove access to the work immediately and investigate your claim.

This work is downloaded from Delft University of Technology.
For technical reasons the number of authors shown on this cover page is limited to a maximum of 10.

Case Studies in Thermal Engineering 54 (2024) 103940

Contents lists available at ScienceDirect

Case Studies in Thermal Engineering

journal homepage: www.elsevier.com/locate/csite

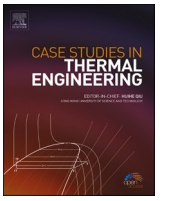

Junction temperature and luminous flux prediction for white LED array based on electrical-photo-thermal modeling

Minne Liu [a,1], Wenyu Li [a,1], Wei Chen [a], Mesfin S. Ibrahim [c], Jingkang Xiong [e], Guoqi Zhang [d], Jiajie Fan [a,b,f,*]

[a] Academy for Engineering & Technology, Fudan University, Shanghai, 200433, China
[b] State Key Laboratory of Applied Optics, Changchun Institute of Optics, Fine Mechanics and Physics, Chinese Academy of Sciences, Changchun, 130033, China
[c] Centre for Advances in Reliability and Safety, New Territories, Hong Kong
[d] Delft University of Technology, 2628, Delft, the Netherlands
[e] Changzhou Institute of Technology Research for Solid State Lighting, Changzhou, 213164, China
[f] Fudan Zhangjiang Institute, Shanghai, 201203, China

ARTICLE INFO

Handling editor: Huihe Qiu

Keywords:
Light-emitting diode
Multiple-chip array
Junction temperature
Luminous flux
Thermal coupling
Electrical-photo-thermal modeling

ABSTRACT

During the operation of an LED array, its thermal and optical performances are always not equal to the superposition of the individual LED's characteristics because of a significant thermal coupling effect between the arrays. Based on this, this paper proposes an electrical–photo-thermal model, with considering both junction temperature and luminous flux, to predict the both the thermal and optical performances of LED arrays operated under different currents, case temperatures, and lighting methods. The junction temperature and luminous flux of a single LED operating under different driving currents and case temperature conditions are firstly collected to establish the luminous flux response surface model of a single chip. Then it is used to predict the luminous flux of an array, whose junction temperature is predicted using both thermal coupling matrix (TCM) and numerical models. Experiments verify the luminous flux of the LED array under different operation conditions and show that the proposed electrical–photo-thermal modeling can be used to predict the thermal and optical parameters of LED arrays with 95 % accuracy. Thus, it is effective for the fast prediction of the junction temperature and luminous flux of large LED systems with array structures, i.e. intelligent automotive lightings and displays.

1. Introduction

From the earliest days of firewood to the current electrical age, lighting is inseparable from our lives. Russian scientist Oleg Losevs produced the first LED. American researcher holonyak invented the first red LED [1]. The innovation of high-brightness red and yellow LEDs and the appearance of high-brightness blue LEDs [2] established the basis for the birth of white LEDs. The principle is to convert part of the blue light into yellow light by combining blue LEDs with phosphors. The superposition produces white light. In the late 1990s, LED manufacturers started to produce white LEDs. The brightness, efficiency and color quality also gradually improved.

White LEDs, as solid-state lighting, are now widely used in different areas of our daily life, such as lighting, including home lighting,

* Corresponding author. Academy for Engineering & Technology, Fudan University, Shanghai, 200433, China.
E-mail address: jiajie_fan@fudan.edu.cn (J. Fan).
[1] They contributed this work equally.

https://doi.org/10.1016/j.csite.2023.103940
Received 21 August 2023; Received in revised form 11 December 2023; Accepted 22 December 2023
Available online 3 January 2024
2214-157X/© 2024 The Authors. Published by Elsevier Ltd. This is an open access article under the CC BY license (http://creativecommons.org/licenses/by/4.0/).

commercial lighting and outdoor lighting. With high efficiency and long life, white LEDs can save energy and reduce maintenance costs compared to traditional incandescent and fluorescent lamps. Also, white LEDs can provide light with different color temperatures and brightnesses to meet the needs of different environments and atmospheres [3]. The high brightness and fast response time of white LEDs have made them ideal for automotive lighting [4]. At the same time LEDs have high efficiency and long life. It can provide brighter and more uniform illumination and reduce energy consumption, while LEDs are used in street and street lighting, home electronics, medical and scientific instruments, and other applications [5–8].

As technology continues to advance, the brightness and efficiency of LEDs continue to improve. The application area of high brightness LEDs extends to various fields such as lighting, display, and automotive lighting. Usually, the input power is converted partly into light energy and partly into thermal energy, but only about 20 % of the energy is converted into light in LEDs, and the remaining energy is converted into thermal energy [9–12] causing an increase in the junction temperature, which further affects the optical performance. Therefore, the luminous efficiency of LEDs always decreases at high temperatures and high currents [13]. To achieve higher luminous flux and lower cost, LEDs are packaged in high current density driven multi-chip package modules [14–16]. In this case, the efficiency degradation effect under high current drive consumes more power. In fact, if the excessive thermal energy generated cannot be eliminated, the high temperature inside the LED and the temperature gradient will not only generate huge pressure along the surface [17,18], but also accelerate the degradation of light output and bring serious catastrophic accidents [19–21]. Therefore, thermal management of multi-chip LEDs (MC LEDs) is necessary to obtain good performance and longer lifetime [22].

In terms of junction temperature prediction, most of the junction temperature predictions are basically based on single-chip LEDs. Shailesh [23] explored the possibility of monitoring and measuring the junction temperature of LEDs in luminaires using the strong correlation between the forward voltage drop at the LED junction and the junction temperature. The results showed that the inherent forward voltage/junction temperature correlation of LEDs can be used to measure and monitor the junction temperature of LEDs in luminaires under operating conditions. E. Ozuturk [24] has been taken advantage of the relative variation of radiant power with junction temperature characteristic of LED to measure junction temperature. The error ratio of the calculated junction temperature decreases in pulsed high currents. Luo [25] implemented the junction temperature prediction of a single Luxeon style packaged LED chip based on an analytical model. Some scholars have made junction temperature prediction based on spectra, Tamura et al. [26] in 2000 pointed out that blue chips and phosphors decay at different rates with increasing temperature. Based on Tamura's work, Gu [14] proposed to use the blue-white ratio to characterize GaN-based white LEDs. The ratio of the total radiant energy (W) of the white LED and the radiant energy of the blue emission spectrum (B) is used as a prediction of the junction temperature. Chen [27] used the central wavelength method to characterize the junction temperature of AlGaInP-based LEDs. scholars such as Lin [28] proposed to use either the center-of-mass wavelength or the half-wave (FWHM) combined with the driving current to characterize the junction temperature of LEDs. Liu [29] analyzed the temperature distribution of the LEDs to understand the relationship between thermal resistance and the position of the LEDs on the aluminium substrate. Structure-function measurements of LEDs placed on aluminium substrates were carried out using a thermal transient tester (T3ster) and an integrating sphere. Guidance was provided to understand the thermal reliability of LED lamps and to design thermal management techniques.

When multiple LED chips are combined to form an LED array, the light emitted by each chip can be absorbed, scattered, and reflected by the surrounding materials, generating heat and affecting the performance and lifespan of the device. In LED array devices, the light emitted by the LED chip is absorbed by the surrounding materials, including the LED chip itself, packaging materials, and substrates. These materials undergo a thermalization process after absorbing the light, generating heat, and thus affecting the temperature distribution and stability of the LED chip [30]. LED chip itself also generates heat, which is transferred to the surrounding materials through thermal conduction, convection, and radiation. Lu addressed the issues in temperature measurement methods for high-power multi-chip LED modules (MCMs) [31,32] and proposed a fast and simplified measurement method for predicting the junction temperature of multi-chip modules in high-power LED systems using a thermal coupling matrix. The proposed method utilizes the Equivalent Electrical Circuit (EEC) approach to establish a thermal coupling matrix model for predicting the junction temperature. Xiao [33] et al. considered the junction temperature of LED car light chips, and used a constant temperature experimental platform and ANSYS Workbench simulation to explore the effects of different factors (chip power, ambient temperature, chip distribution spacing, and chip distribution shape) on the junction temperature of LED car light chips.

Chen [34] also employed the equivalent circuit approach to simulate the lateral heat coupling effect in LED arrays and predicted the junction temperature distribution of the LED array using a thermal coupling matrix. Tang [35] conducted a numerical investigation on the heat transfer performance of a multi-chip (MC) LED module using a general analytical solution. Pohl et al. [36,37] proposed a numerical algorithm called "trace of photothermal flux" to solve the 3D heat conduction problem, which includes simulating the thermal effects (heat transfer and generation) in the substrate and phosphor, as well as tracking the propagation and absorption of light. This method was ultimately validated by using LED packaging samples with known phosphor ratios and parameters (conversion efficiency at different temperatures).

In the prediction of optical performances for white LED，Hui et al. [38] connected the emission, electrical, and thermal aspects of LED systems. The theoretical model can be used to predict the optimal operating point for LED systems to achieve maximum luminous flux under specific thermal conditions. Based on this theoretical model, it can also explain why the maximum luminous flux of an LED system may not occur under rated power conditions, and experimental validation has been conducted to support this theory. Based on this theory, they [39] provided a tutorial on LED system theory based on the extended PET theory. This tutorial provides materials for electronics engineers with switched mode power supply design background for optimal LED system designs, such as k_h ， k_c. Bin-Juine Huang et al. [40] proposed a thermal-electrical-optical model for multi-chip multicolor lighting appliances for illumination control. Jeong Park [41] et al. investigated the effect of current diffusion layer and junction temperature on LED characteristics by combining

the electrical and optical properties of GaN/InGaN multi-quantum well sapphire light-emitting diodes, which can be specifically derived from the effect of series resistance The effect of heat generation and junction temperature increase on the LED efficiency can be specifically derived.

All three parameters of the photoelectricity and heat of LEDs exist in an interactive and interrelated relationship, which has been described in the theory of photoelectricity and heat (PET) [42]. The LED models that exist provide a clear understanding of the working mechanism and the whole process of electroluminescence and heat dissipation, but the heat transfer process is more complex when the LED array is working than when a single chip LED is working independently. The thermal coupling process is more complex [38]. Especially in high-power LED array systems, the LED array temperature distribution is more influenced by the chip next to it due to the thermal coupling effect, so it is not possible to use the photothermal equation of single-chip LEDs directly. Most of the current research is focused on for single WLED packages, or the study of LED thermal coupling effect, few have combined the two, in predicting the optical performance of LED arrays while considering the thermal coupling effect between LED arrays.

In order to realize the optical performance of LED arrays under different driving currents and temperatures, the thermal coupling heat transfer process of LED arrays is analyzed, and an optical-thermal-electric model combining junction temperature prediction model and luminous flux prediction model is proposed. The junction temperature prediction is performed by the TCM matrix model and numerical algorithm model, respectively, considering the thermal coupling effect inside the LED array. The developed luminous flux model models a single LED and then on the LED array. The luminous flux model is combined with the junction temperature prediction model to predict the optical and thermal parameters of the LED array under different lighting methods by inputting the driving current, thermal power, and temperature. Finally, the accuracy of the proposed, optical-thermal-electric model is verified under different operating conditions. The rest of the paper is organized as follows: Section II presents the test samples and experiments involved in this paper as well as the luminous flux response model. Section III presents the junction temperature and luminous flux prediction models for the LED array modules. Section IV focuses on the accuracy of these model predictions. The last section gives concluding remarks.

2. Single chip tests and modeling

This section introduces the LED samples and the test protocols involved in the experiments. The experiments include surface temperature tests, junction temperature tests and optoelectronic parameter tests under variable temperature and current conditions.

2.1. Test sample's introduction

The sample selected for this study is LUXEON Neo CW (0.5 mm^2) LED single bead from Lumileds, as shown in Fig. 1.

The main structure of the LED bead includes the phosphor on the top of the die, the polarity mark to distinguish the cathode from the anode by welding on the current, the side coating to protect the package structure, the embedded Transient Voltage Suppressor (embedded Transient Voltage Suppressor), the Optical Character Recognition (Optical Character) to distinguish the chip type, and the electrical pad of the cathode. The LED chip area is 0.5 mm^2. The light-emitting area is 0.76 mm * 0.76 mm. The package size is 1.13 mm*1.13 mm. The rated voltage and rated current of LUXEON Neo CW 0.5 mm^2 LED are 3.13V and 350 mA respectively. Fig. 1(c) shows the package of a single bead module. The PCB is an aluminum substrate copper clad board with size 10 mm * 10 mm and thickness 1.6 mm.

The experimental sample of the LED array module and the configuration of the 3-D LED module are shown in Fig. 2. The module consists of 84 beads connected in series to form an LED array. The module beads are exactly the same as the single module sample. In the experiment, nine LEDs were selected as the smallest component unit of the LED array (3 * 3 LED array), and different lighting modes of the LED array module were realized by short-circuiting the wires. Array experiments involving the lighting mode shown in Fig. 3 include six cases: (a) four all illuminated (b) interval four all illuminated (c) diagonal two (d) side by side two illuminated (e) six all illuminated (f) nine all illuminated. These six lighting situations are named: Sample 1, Sample 2, Sample 3, Sample 4, Sample 5, Sample 6, to facilitate subsequent differentiation.

2.2. Experimental setups and tests

The test protocols were designed to obtain the parameters of junction temperature and luminous flux for the single LED bead module of LUXEON Neo CW 0.5 mm2 type in Fig. 1 and the LED array with different lighting methods in Fig. 2. Table 1 lists the test

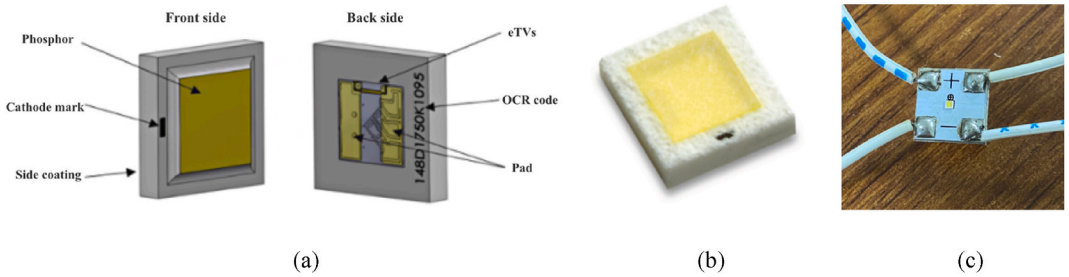

Fig. 1. LUXEON Neo CW 0.5 mm2 type LED: (a) LED structure diagram; (b) chip object diagram; (c) package single bead module.

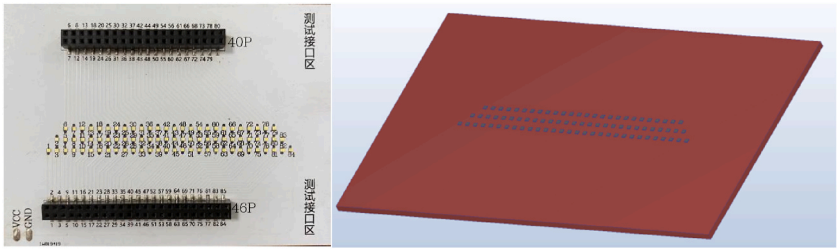

Fig. 2. LED Array Module: (a) LED Module test sample; (b) 3-D configuration.

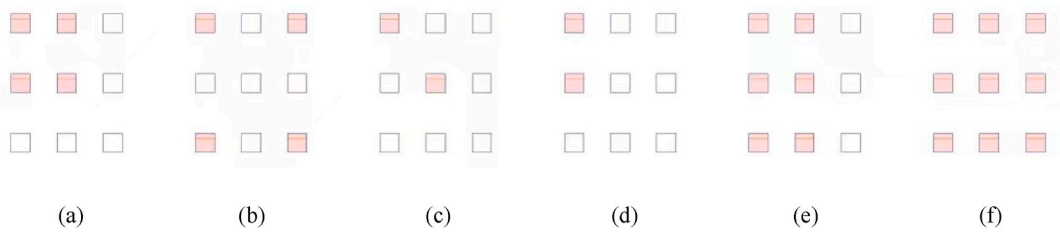

Fig. 3. 6 types of LED array lighting mode.

protocols for the samples at different currents and different case temperatures. This scheme will also be used to build the relationship between luminous flux and the junction temperature.

2.2.1. Junction temperature and surface temperature testing

To ensure the accuracy of the experiments, all experiments were conducted in a windproof chamber and the ambient temperature was controlled to 27 °C.

The junction temperature was measured by a Leeds junction temperature measuring instrument (LEETS LEDT-300B, with the error of K-factor within ±0.5 and the error of junction temperature within ±1 °C). The junction temperature test equipment includes: data acquisition computer, LEETS junction temperature measuring instrument, heating oven (ESPEC, ST-110), DC power supply (KEYSIGHTN 5751) and temperature control heating platform, as shown in Fig. 4. The forward voltage method for junction temperature measurement consists of two parts: calibration and measurement. The calibration part is mainly to obtain the coefficient relationship of K. The test part uses a temperature-controlled platform to keep the case temperature of the sample constant. Thermal grease is used to ensure effective thermal conductivity between the sample and the heating platform. Also a clamp is used to place the LED samples on the temperature control platform.

2.2.2. Photo-electric paraments measurement

The single LED and LED array modules were used to collect the optoelectronic parameters using integrating spheres (Model: EVERFINE HASS20) with a radius of 0.5 m and 2 m, respectively, a DC power supply (Model: KEYSIGHT N5717), a thermal control platform system, and a computer. The integrating sphere was calibrated using the EVERFINE SLD062 and SLD204 universal standard light source calibration lamps, respectively, and was calibrated separately before each test. The test sample is fixed on the temperature-controlled platform with silicone grease, and the data is collected after waiting for 10 min to reach the thermal equilibrium state. Fig. 5 shows the LED optoelectronic parameter testing system.

Table 1
Single LED and LED module test set-up.

Test Type	Sample Type	Test Setup	Sample Numbers
Optical and electrical parameter tests	Single LED	Operating current: 150mA–500mA Gradient: 50 mA; Module Case Temperature: 40°C–90 °C Gradient:10 °C.	3
	LED Array Module	Operating current: 100 mA, 200 mA, 300 mA, 600 mA Module Case Temperature: 40 °C, 60 °C.	2
Junction temperature test	Single LED	Operating current: 150mA–500mA Gradient: 50 mA; Module Case Temperature: 40°C–90 °C Gradient: 10 °C.	3

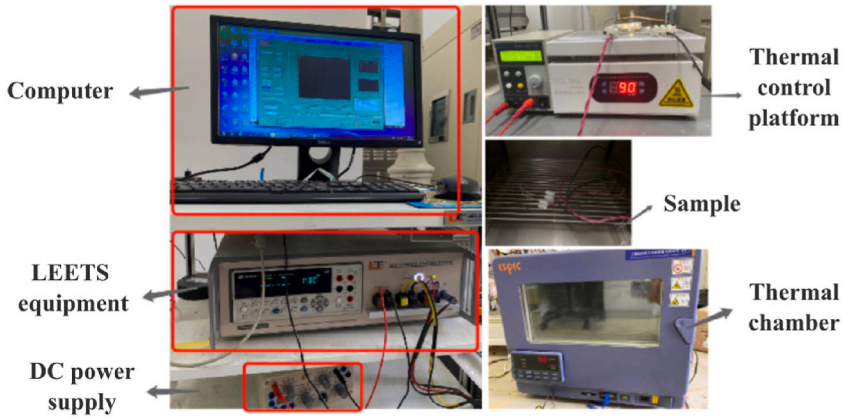

Fig. 4. Junction temperature test system.

2.3. Luminous flux modeling

LED luminous flux is affected by current and temperature. As the current increases, the thermal power will increase, resulting in a rise in luminous flux. The heat generated by the chip is also increasing. It would lead to a decrease in the luminous efficiency of the LED components; thus, the light efficiency of the chip would be degraded. In order to predict the luminous flux of a single LED and LED array under different operating conditions, a luminous flux response surface model is proposed [43]. This Model I, is shown in Equation (1):

$$\Phi\left(I_f, T_j\right) = \Phi_{v_0}\left(\frac{I_f}{I_{f_0}}\right)^{D} e^{ln(HC)\left(\frac{T_j - T_{j_0}}{75}\right)} \tag{1}$$

Where HC thermal cooling coefficient indicates the degree of the change of light efficiency with junction temperature. D indicates the variation of luminous efficiency with current. I_{f_0}, T_{j_0} and Φ_{v_0} indicate the rated driving current, rated operating temperature, and luminous flux at the rated driving current and operating temperature.

Model I can describe the luminescence of phosphor-converted white LEDs very well. However, in extreme scenarios, Model I is not able to capture the LED luminescence accurately. Model I is not suitable for high luminous efficacy, very low current, high power and high luminous flux scenarios. Based on that, Model II is proposed to predict the LED luminous flux over a wide range of current variations accurately:

$$\Phi\left(I_f, T_j\right) = \Phi_{v_0}\left(\frac{I_f}{I_{f_0}}\right)^{\left(D + C_e\ ln\left(\frac{I_f}{I_{f_0}}\right)\right)}\left(\alpha_1 - \alpha_2 n^{\left(\frac{T_j - T_{j_0}}{100 - T_{j_0}}\right)}\right) \tag{2}$$

α_1 and α_2 are obtained from the following equations:

$$\alpha_1 = 1 + \alpha_2 \tag{3}$$

$$\alpha_2 = \frac{HC\left(\mathrm{I}_f\right) - 1}{1 - n} \tag{4}$$

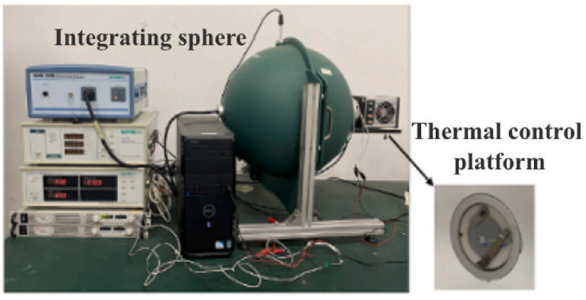

Fig. 5. Single LED photoelectric parameter testing system.

$$\alpha_3 = \left(\frac{m + \mathrm{I}_{f_0}}{\mathrm{I}_{f_0}}\right) \tag{5}$$

$$HC(\mathrm{I}_f) = HC_0 \bullet \alpha_3 \bullet \left(\frac{\mathrm{I}_f}{m + \mathrm{I}_f}\right) \tag{6}$$

Where HC_0 is the nominal *HC* factor. m is the current factor of *HC*. n is the temperature power factor of the luminous flux.

$$HC_0 = \frac{\Phi_v\left(I_{f_0}, T_j = 100^{\circ}C\right)}{\Phi_v\left(I_{f_0}, T_{j_0}\right)} \tag{7}$$

The improved Model II improves the current variation range compared to Model I by introducing the $D + C_e\, ln\left(\frac{I_f}{I_{f_0}}\right)$ and $HC(I_f)$ functions. $G(x) = \alpha_1 - \alpha_2 n^{\left(\frac{T_j - T_{j_0}}{100 - T_{j_0}}\right)}$ is also introduced to increase the prediction accuracy under junction temperature conditions.

3. Electrical-photo-thermal modeling for multiple chip array

3.1. Junction temperature modeling

In this section, a thermal-electrical model is built to predict the junction temperature of the LED array model by inputting thermal power and driving current. The model takes the thermal coupling phenomenon into account.

3.1.1. Thermal coupling matrix model

3.1.1.1. 1 Theory and models. When the LED is illuminated on a thermostatic platform, the heat dissipated from above can be ignored. The heat dissipation path is conducted from the LED chip downward. According to the thermal resistance theory, the equivalent thermal resistance model is shown in Fig. 6(a). The junction temperature of a single LED under different driving currents can be obtained from the thermal resistance, as shown in equation (8):

$$T_j = T_c + \Delta T = T_c + P_i \times R = T_c + P_i \times (R_1 + R_2 + R_3) \tag{8}$$

Where T_c is the temperature of the temperature control platform. P_i is the thermal power. Equivalent substitution R indicates the thermal resistance of LED_i. At the same time, R_1 denotes the heat transfer thermal resistance between the LED chip and the PCB board. R_2 denotes the heat transfer thermal resistance between the PCB board and the temperature control platform. And R_3 the convection resistance between the heat sink and the environment.

In the LED array according to Fig. 6(b), P_1 , P_2 , P_3… P_j are the thermal power generated by each LED respectively. R_{ij} is the equivalent thermal resistance between the i-th LED and the j-th LED. For the i-th LED, the temperature rising due to P_i can be expressed as $\Delta T_{ii} = R_{ii} \times P_i$. If the j-th LED transfers the η_{ij} lateral thermal path of the total thermal power P_j to the i-th LED, the temperature rise of the i-th LED can be expressed as its own temperature rise combined with the lateral temperature rise, which is:

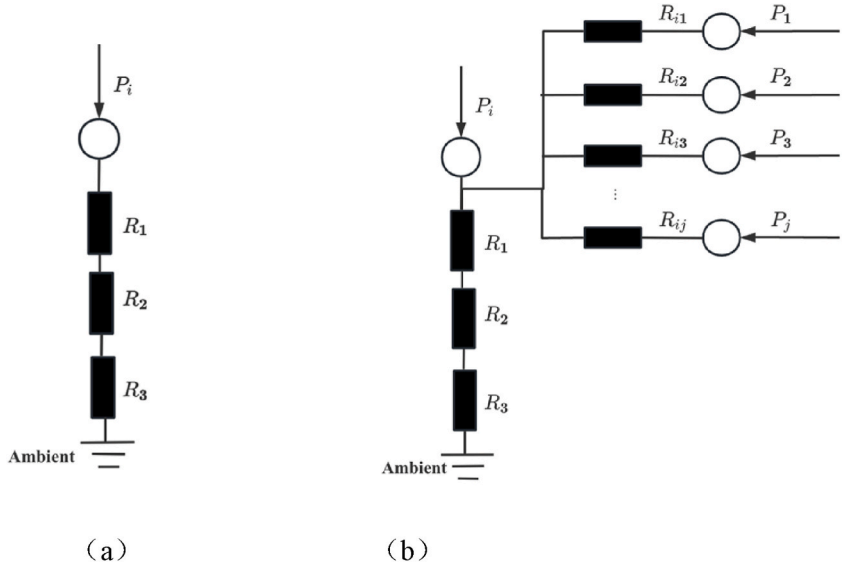

Fig. 6. LED heat transfer model: (a) Single LED (b) LED array.

$$\Delta T_i = \Delta T_{ii} + \sum_{j=1,j\neq i}^{n} \Delta T_{ij} = \sum_{j=1}^{n} \mu_{ij} P_j \tag{9}$$

Where $\mu_{ij} = \eta_{ij} \times R_{ij}$ and $\eta_{ii} = 1$. This parameter is the thermal coupling coefficient, reflecting the degree of thermal coupling, the coefficient μ is a constant value when the structure and material of the LED array is determined. Then the temperature rise can be expressed in a matrix as:

$$\begin{bmatrix} \Delta T_1 \\ \Delta T_2 \\ \Delta T_3 \\ \vdots \\ \Delta T_n \end{bmatrix} = \begin{bmatrix} R_1 & \mu_{12} & \mu_{13} & \cdots & \mu\,1n \\ \mu_{21} & R_2 & \mu_{23} & \cdots & \mu_{2n} \\ \mu_{31} & \mu_{32} & R_3 & \cdots & \mu_{3n} \\ \vdots & \vdots & \vdots & \cdots & \vdots \\ \mu_{n1} & \mu_{n2} & \mu_{n3} & \cdots & R_n \end{bmatrix} \begin{bmatrix} P_1 \\ P_2 \\ P_3 \\ \vdots \\ P_n \end{bmatrix} \quad \text{or}$$

$$\Delta \overrightarrow{T} = \overrightarrow{U_{TCM}\,\overrightarrow{P}} \tag{10}$$

The junction temperature of the matrix can be expressed as Eq. (11):

$$\overrightarrow{T_j} = \overrightarrow{T_c} + \Delta \overrightarrow{T} \tag{11}$$

3.1.1.2. Simulation of TCM model. The model is based on a finite element thermal simulation performed using natural convection dissipation in Autodesk CFD 2023 to estimate the temperature of the sample. To derive the TCM rules and verify the thermal coupling between any two chips in the LED array, the simulation is performed on the 3*3 chip model shown in Fig. 7. The dies are labeled as LED*1#, 2#, 3#, 4#, 5#, 6#, 7#, 8#, 9#* from left to right and top to bottom. The key parameters used for simulation (including thermal resistance and key materials) are listed in the table, as shown in Tables 2 and 3.

$$\begin{bmatrix} T_{j1} \\ T_{j2} \\ T_{j3} \\ T_{j4} \\ T_{j5} \\ T_{j6} \\ T_{j7} \\ T_{j8} \\ T_{j9} \end{bmatrix} = T_c + \begin{bmatrix} 96.99 & 0.73 & 0.23 & 0.51 & 0.34 & 0.15 & 0.12 & 0.10 & 0.06 \\ 0.73 & 96.98 & 0.73 & 0.34 & 0.51 & 0.34 & 0.10 & 0.13 & 0.10 \\ 0.23 & 0.73 & 96.06 & 0.15 & 0.33 & 0.51 & 0.06 & 0.10 & 0.12 \\ 0.51 & 0.34 & 0.15 & 97.09 & 0.73 & 0.23 & 0.50 & 0.34 & 0.15 \\ 0.34 & 0.51 & 0.33 & 0.73 & 97.1 & 0.73 & 0.34 & 0.51 & 0.34 \\ 0.15 & 0.34 & 0.51 & 0.23 & 0.73 & 97.08 & 0.15 & 0.34 & 0.51 \\ 0.12 & 0.10 & 0.06 & 0.50 & 0.34 & 0.15 & 96.96 & 0.73 & 0.23 \\ 0.10 & 0.13 & 1.6 & 0.34 & 0.51 & 0.34 & 0.73 & 96.91 & 0.74 \\ 0.06 & 0.10 & 0.12 & 0.15 & 0.34 & 0.51 & 0.23 & 0.74 & 96.98 \end{bmatrix} \begin{bmatrix} P_1 \\ P_2 \\ P_3 \\ P_4 \\ P_5 \\ P_6 \\ P_7 \\ P_8 \\ P_9 \end{bmatrix} \tag{12}$$

The temperature rise for LED1# can be expressed as $\Delta T_1 = \mu_{11}P_1 + \mu_{12}P_2 + \mu_{13}P_3 + \mu_{14}P_4 + \mu_{15}P_{5+}\mu_{16}P_6 + \mu_{17}P_7 + \mu_{18}P_8 + \mu_{19}P_9$. By holding the other LED power constant, μ_{12} can be obtained through the fitting curve with measured ΔT_1 under various P_2 , as shown in Fig. 8. Fig. 8(a) represents the variation of ΔT_2 to ΔT_9 with LED*1#* thermal power, and the slope corresponds to the matrix coefficients, μ_{ij} can be derived by $\Delta T_i \sim P_j$, the residual matrix coefficients can be obtained. Fig. 8(b) represents μ_{11}, the slope of ΔT_1 variation with P_1. In order to verify the TCM matrix, the process followed for the mutual thermal coupling between any two chips is described in the flow diagram (shown in Fig. 9). Eventually, the ninth-order TCM of sample 6 can be expressed as:

3.1.2. Numerical model

Since thermal coupling will directly affect the junction temperature of the chip when multiple LEDs are illuminated, the thermal

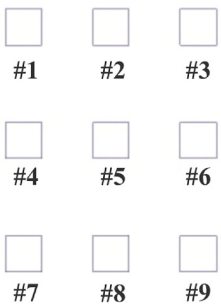

Fig. 7. 3*3 LED array for simulation.

Table 2
The assumed thermal resistance used in the simulation.

Items	Descriptions
Thermal resistance of LED	From the junction to the PCB including the solder layer: 28K/W
Thermal contact resistance 1	Between the underside of the LED and upside of PCB: 0.65 cm2 ·K/W
Thermal contact resistance 2	Between the underside of the PCB and Surface of the temperature control platform：0.77 cm2·K/W

Table 3
The key material parameters used in the simulation.

Materials	Density (g·cm-3)	Thermal conductivity (W/(cm·K))	Heat Capacity (J/g·K)
Air	/	2.563 × 10-4	1.004
PCB	4.75	1.55	0.43

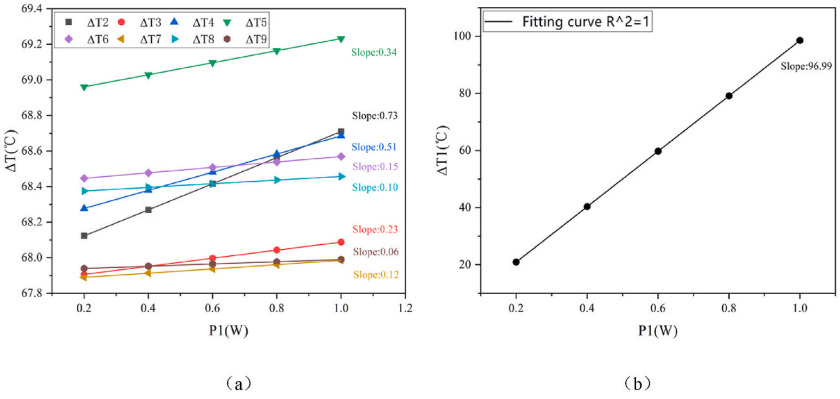

Fig. 8. (a) Δ*T*2, Δ*T*3, Δ*T*4, Δ*T*5, Δ*T*6, Δ*T*7, Δ*T*8, Δ*T*9 VS P_{th} of *1*st LED; (b) Δ*T*1 VS P_{th} of *1*st LED.

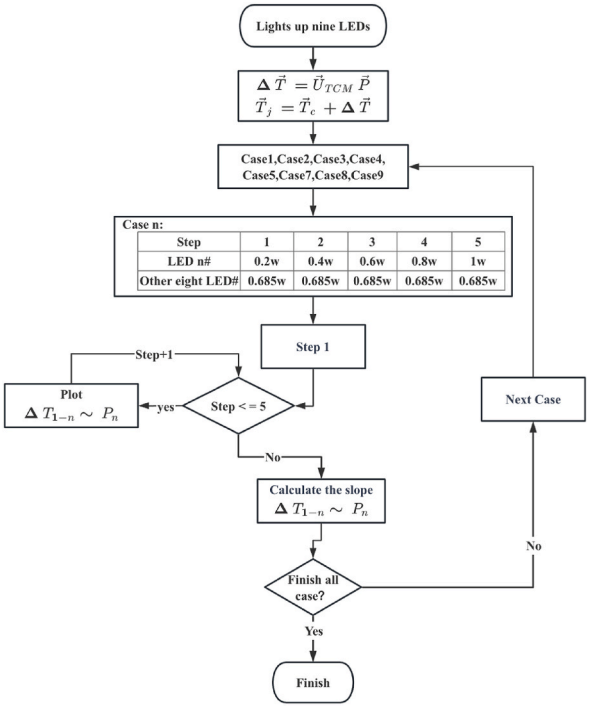

Fig. 9. The mutual thermal coupling calculation scheme of the random chips in the 3*3 LED array.

coupling phenomenon needs to be modeled separately. The steady-state Laplace equation for heat transfer is expressed as follows:

$$\nabla^2 T = \frac{\partial^2 T}{\partial x^2} + \frac{\partial^2 T}{\partial y^2} + \frac{\partial^2 T}{\partial z^2} = 0 \tag{13}$$

Where the coordinate axis takes the upper surface corner of the substrate as the origin. The positive direction of z-axis points to the heat conduction direction, as shown in Fig. 10. The size of the substrate is $L_x * L_Y$. The size of the LED is $a * b$. The coordinates of the center point of the LED are (X_c, Y_c). The thickness of the structure is t.

It is assumed that the substrate is insulated all around. The bottom side holds the temperature constant T_0. The top surface has heat input only in the area covered by the chip with the other locations set as adiabatic boundaries. Under these boundary conditions, the temperature distribution at each location when a single chip is heated can be solved as:

$$\theta(x,y,z) = A_0 + B_0(z-t) + \sum_{m=1}^{\infty} cos(\lambda x)[A_1\ cosh(\lambda z) + B_1\ sinh(\lambda(z-t))]$$

$$+ \sum_{n=1}^{\infty} cos(\delta y)[A_2\ cosh(\delta z) + B_2\ sinh(\delta(z-t))]$$

$$+ \sum_{m=1}^{\infty}\sum_{n=1}^{\infty} cos(\lambda x)cos(\delta y)[A_3\ cosh(\beta z) + B_3\ sinh(\beta(z-t))] \tag{14}$$

$$\varphi(\xi) = \frac{k\xi A_s}{-Q}\theta_0 \tag{15}$$

$$B_1 = \frac{\int_0^{L_x} \frac{\partial\theta}{\partial z} \bullet \frac{1}{\lambda} \bullet cos(\lambda x)dx}{cosh(\lambda t)\int_0^{L_x} cos^2(\lambda x)dx} \tag{16}$$

$$B_2 = \frac{\int_0^{L_y} \frac{\partial\theta}{\partial z} \bullet \frac{1}{\delta} \bullet cos(\delta y)dy}{cosh(\delta t)\int_0^{L_y} cos^2(\delta y)dy} \tag{17}$$

$$B_3 = \frac{\int_0^{L_x}\int_0^{L_y} \frac{\partial\theta}{\partial z} \bullet \frac{1}{\beta} \bullet cos(\lambda x)cos(\delta y)dxdy}{cosh(\beta t)\int_0^{L_x}\int_0^{L_y} cos^2(\lambda x)cos^2(\delta y)dxdy} \tag{18}$$

$$A_o = T_0 \tag{19}$$

$$B_o = -\frac{Q}{kL_x\ L_Y} \tag{20}$$

Where $\theta(x,y,z) = T(x,y,z) - T_f$, $\lambda = m\pi/L_x$, $\delta = n\pi/L_y$, $\beta = \sqrt{\lambda^2+\delta^2}$ and $A_i = \varphi(\xi)B_i$. The thickness of the substrate is t. And the thermal conductivity of the material is k. The thermal power generated by the LED is Q. θ states the temperature rise. T_f states the ambient temperature.

Due to the linear superposition property of the heat conduction, the temperature distribution of multiple heat sources applying to the substrate can be expressed as:

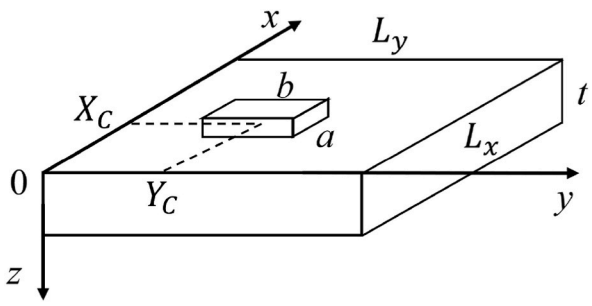

Fig. 10. Isotropic plate with single heat source.

$$\theta_{sum}(x,y,z) = \sum_{i=1}^{n} \theta_i(x,y,z) \tag{21}$$

With the ambient temperature overlaying, the temperature distribution on the substrate of multi-sources is expressed as:

$$T_{sum}(x,y,z) = \theta_{sum}(x,y,z) + T_{air} = \sum_{i=1}^{n} \theta_i(x,y,z) + T_{air} \tag{22}$$

3.2. Luminous flux modeling

The luminous flux prediction model for the LED array is shown in Fig. 11.

First, the junction temperature of each LED is predicted by the model in 3.1 for LED arrays with different lighting methods, driving currents, and temperatures. Then, after the junction temperature of each LED is obtained, the luminous flux of the LED array is obtained by superimposing each LED luminous flux according to the Luminous flux modeling of single LED in 2.3.

4. Results and discussion

4.1. Junction temperature modeling

4.1.1. Validation of TCM model

The ninth order TCM matrix of sample 6 at a case temperature of 60 °C is obtained by FEM simulation. The FEM simulation is performed at a drive current of 0.2 A. A comparison of the finite element simulation results and the TCM model predictions using equation (12) is shown in Fig. 12.

Under the same conditions, the finite element simulation of sample 1 (Fig. 3(a) with all four illuminated cases) is used to verify the applicability of the TCM model when part of the LEDs in the array are lighted. The input thermal power of the remaining five unlit lights is 0w, and the input power of *1#, 2#, 4#* and *5#* is 0.46w each, as shown in Equation (23):

$$\begin{bmatrix} T_{j1} \\ T_{j2} \\ T_{j3} \\ T_{j4} \\ T_{j5} \\ T_{j6} \\ T_{j7} \\ T_{j8} \\ T_{j9} \end{bmatrix} = 60 + \begin{bmatrix} 96.99 & 0.73 & 0.23 & 0.51 & 0.34 & 0.15 & 0.12 & 0.10 & 0.06 \\ 0.73 & 96.98 & 0.73 & 0.34 & 0.51 & 0.34 & 0.10 & 0.13 & 0.10 \\ 0.23 & 0.73 & 96.06 & 0.15 & 0.33 & 0.51 & 0.06 & 0.10 & 0.12 \\ 0.51 & 0.34 & 0.15 & 97.09 & 0.73 & 0.23 & 0.50 & 0.34 & 0.15 \\ 0.34 & 0.51 & 0.33 & 0.73 & 97.1 & 0.73 & 0.34 & 0.51 & 0.34 \\ 0.15 & 0.34 & 0.51 & 0.23 & 0.73 & 97.08 & 0.15 & 0.34 & 0.51 \\ 0.12 & 0.10 & 0.06 & 0.50 & 0.34 & 0.15 & 96.96 & 0.73 & 0.23 \\ 0.10 & 0.13 & 1.6 & 0.34 & 0.51 & 0.34 & 0.73 & 96.91 & 0.74 \\ 0.06 & 0.10 & 0.12 & 0.15 & 0.34 & 0.51 & 0.23 & 0.74 & 96.98 \end{bmatrix} \begin{bmatrix} 0.46 \\ 0.46 \\ 0 \\ 0.46 \\ 0.46 \\ 0 \\ 0 \\ 0 \\ 0 \end{bmatrix} \tag{23}$$

Junction temperature of the sample 1 array and finite element simulation results are shown in Fig. 13.

From Figs. 12 and 13, it can be seen that the error is within 0.0015 % between the finite element simulation results and the TCM results. It indicates that the TCM model can be applied to predict the junction temperature under different case temperature, driving current conditions and different LED array lighting methods without FEM simulation. From the TCM model, it can be concluded that 1) μ is only related to the distance. The coefficient influence would shrink while the distance enlarges; 2) the TCM matrix is a symmetric matrix, $\mu_{ij} = \mu_{ji}$. 3) The TCM can also be used for junction temperature prediction when the LED array is partially lightened with random modes.

4.1.2. Numerical model application

The connection between the LED chips is the air and the PBC substrate. The convection heat exchange capacity of air is weak, so it is reasonable to analyze the thermal coupling in the PCB where the vertical thermal conduction only exists. With the same chip parameters and input power, the temperature rise caused by the thermal resistance of each chip above the substrate is also the same. In order to verify the accuracy of numerical modeling in 3.1.2, the matlab simulation settings in Fig. 12 are adopted. The temperature

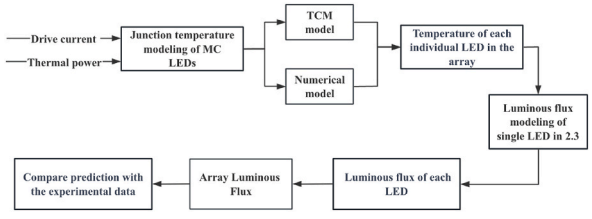

Fig. 11. LED array luminous flux prediction scheme.

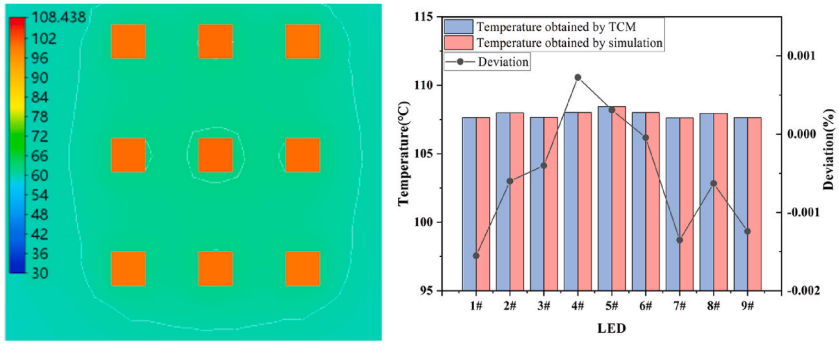

Fig. 12. LED array junction temperature prediction under case temperature 60 °C and driving current 0.2A: (a) finite element simulation results (b) result comparison.

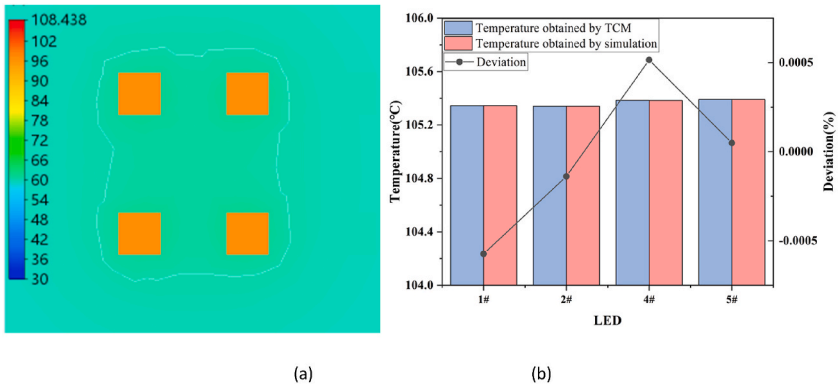

Fig. 13. Junction temperature prediction of LED array under lighting mode Fig. 3(a): (a) finite element simulation results (b) comparison of results.

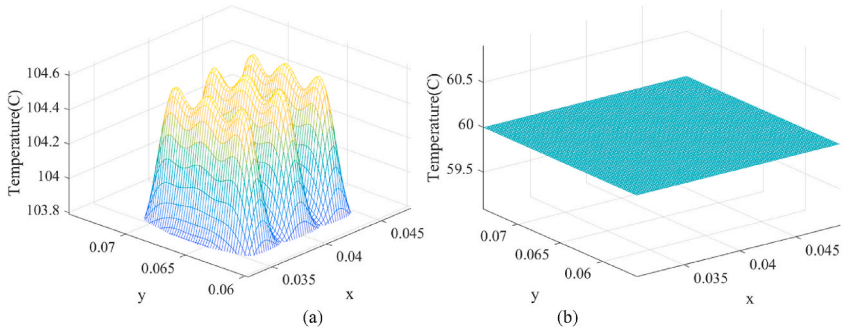

Fig. 14. The temperature distribution of the LED array area (a) on the top surface of the PCB; (b)on the bottom surface of the PCB.

distribution on the top surface of sample 6 is shown in Fig. 14. As the numerical thermal modeling goes, the bottom side of the PCB is the junction temperature of each die is summarized and analyzed in Table 4.

It is obvious to see the multiple temperature peaks generated when 9 LEDs are lighted at the same time. Due to the larger chip pitch in x-axis than in y-axis, the thermal coupling effect is weaker with a wider low temperature region between adjacent chips. The

Table 4
Numerical Junction temperature modeling comparison (sample 6).

Model (°C)		1#	2#	3#	4#	5#	6#	7#	8#	9#
Numerical method	104.43	104.48	104.43	104.46	104.52	104.47	104.43	104.48	104.43	
TCM	107.63	107.98	107.66	108.02	108.44	108.02	107.61	107.95	107.63	

temperature predicted by numerical mothed is 3 °C lower than TCM generally. This difference comes from the absence of contact thermal resistance in the numerical model due to the boundary conditions, which requires the continuous temperature changes. The step temperature rise generated by the contact thermal resistance between the LED and the solder and between the PCB and the temperature control platform can be superimposed directly at the end of the calculation. The precision of the calculation has a significant impact on the results. The junction temperature and computation time of Fourier iterations 10 times, 30 times, 50 times, 80 times in steps of 100e-5 m, 50e-5 m, 20e-5 m are compared for a single chip with 0.5w input power, respectively.

It can be seen from Table 5 that the number of Fourier iterations determines the degree of waveform flatness. The calculation step size determines the accuracy of the evaluation. The step length has no effect on the calculation of temperature, but the number of iterations has an influence on the temperature. The temperature junction temperature increases with the number of iterations.

The TCM model is suitable for junction temperature prediction of fixed samples at different case temperature and current. The process of solving the TCM matrix is time-consuming, with sixty iterations taking approximately 7 min to obtain a single figure, and obtaining the slope of a single LED requires at least five different power simulations. If the LED array contains n samples, $5 * n$ simulations are required, taking $35 * n$ minutes. However, after obtaining the TCM matrix, fast predictions can be made under different scenarios without re-simulation. The numerical calculation method can also characterize the junction temperature prediction results. The calculation time and accuracy will rise with the increase of Fourier series. The computational speed is faster than the TCM matrix solution process for different LED arrays samples, however, it is slower than the same sample under various modes with known TCM matrix.

4.2. Luminous flux model

4.2.1. Flux response surface model of single chip

After completing the electrical-photo-thermal data acquisition, the luminous flux and junction temperature at different currents and different shell temperatures were obtained. The fitting results of Model I and II using the data of three single LED chip samples are shown in Figs. 15 and 16, respectively. The parameters extracted of the two models are listed in Tables 6 and 7.

From the results of the simulation, it can be seen that both Model I and Model II fit well. However, the improved luminous flux response surface model adds three parameters: n, m, and C_e. The R^2 of Model II is slightly higher than that of Model I. Both Model I and Model II can be used for luminous flux prediction. But it is notable that Model II is more accurate for extreme conditions compared to Model I. The improved luminous flux response surface model is more suitable for capturing and describing the luminous flux of LED products under different operating conditions. When D is close to 1, it indicates that the luminous flux varies linearly with the current. The smallest D for #LED2 in Models I and II indicates that the luminous efficiency of #LED2 decreases more severely with the increase of current.

4.2.2. Luminous flux model of multiple chip array validation with case

The junction temperature of the sample 1 array at a driving current of 0.2A and a case temperature of 40 °C can be obtained from 4.1. By substituting the junction temperature and driving current into the luminous flux response surface model, luminous fluxes of the arrays can be obtained by superimposing each LED luminous fluxes in both cases. The predicted results are compared with the experimentally obtained results as shown in Table 8.

$$Deviation = \frac{predicted\ Luminous\ Flux(LED\ array) - Expermental}{Expermental} \times 100\% \tag{24}$$

The results of samples 2, 3, 4, 5, and 6 at 40 °C are also compared with the experiments, respectively. The outcomes are shown in Fig. 17.

It can be seen from Fig. 17 that the luminous flux of Model II is more accurate than that of Model I, which verifies the conclusion that Model II in 4.2.1 is more applicable to extreme conditions. The predicted luminous fluxes are all higher than the experimentally measured luminous fluxes, which may be related to the very small amount of light loss from the LEDs that may be due to the collision of photons in space resulting in a decrease in energy and thus a slight decrease in luminous flux. As the number of samples increases, the overall model error increases. On the one hand, there are differences between samples, and on the other hand, the overall model error is the result of the individual sample error and superposition. It is also evident from the three samples of a single LED that there is a certain difference in luminous flux between samples under the same conditions. In the case of 60 °C shell temperature and 0.2A current, the luminous flux of a single LED is 56.83 ml, and the average luminous flux of each LED in samples 1, 2, 3, 4, 5 and 6 is smaller than that of a single LED, indicating that there is a coupling effect of the LED array, of which sample 6 has the most obvious reduction in luminous flux and the most serious coupling phenomenon. As the spacing of LEDs decreases, the thermal coupling effect is enhanced and the LED temperature rises; as the number of LEDs in the LED array module increases, the thermal coupling effect is enhanced and the LED temperature rises significantly.

5. Conclusion

In this paper, the junction temperature and luminous flux of individual LEDs operating at different drive currents and case temperatures are firstly collected, and a surface model of the luminous flux response of individual chips is established. Thermal coupling analysis and junction temperature prediction of array LEDs are carried out by TCM model and numerical algorithm model, and the difference between the two predictions is very small, but the numerical algorithm model can greatly speed up the operation speed and efficiency. The junction temperature, drive current and case temperature of each LED obtained from the junction temperature

Table 5
Numerical Junction temperature with different Fourier iterations and steps.

Steps length		Fourier iterations			
		10 times	30 times	50 times	80 times
100e-5m	LED Part	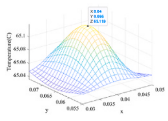	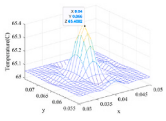	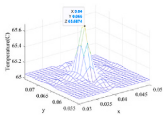	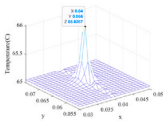
	Overall baseplate	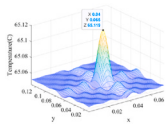	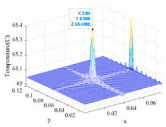	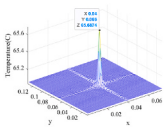	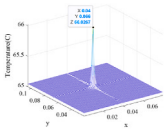
	Tj	65.119 °C	65.4 °C	65.69 °C	66.02 °C
	Time	0.576s	3.07s	7.30s	18.37s
50e-5m	LED Part	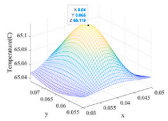	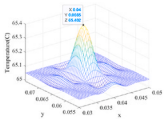	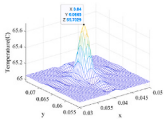	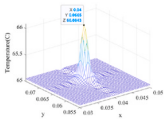
	Overall baseplate	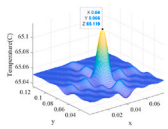	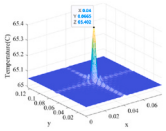	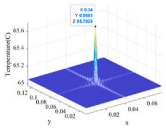	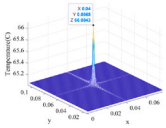
	Tj	65.12 °C	65.4 °C	65.7 °C	66.10 °C
	Time	2.15s	12.62s	31.2s	73.96s
20e-5m	LED Part	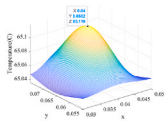	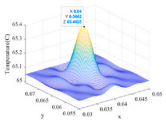	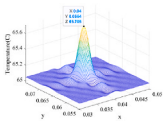	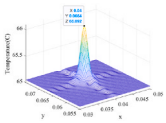
	Overall baseplate	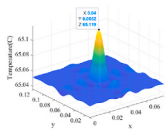	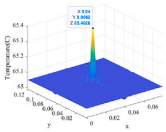	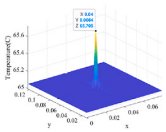	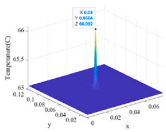
	Tj	65.12 °C	65.4 °C	65.7 °C	66.09 °C
	Time	12.48s	73.79s	188s	477s

prediction model are substituted into the luminous flux response surface model, and the error of Model II is within 5 % compared with the experimentally measured luminous flux. The results show that: 1) the luminous flux response surface model can predict the luminous flux of individual LEDs very well, and for LED arrays, the junction temperature will increase due to thermal coupling, and the accuracy of Model II is higher than that of Model I, which indicates that Model II can also be used in extreme conditions; 2) the TCM model and numerical algorithm model predict the junction temperature with high accuracy, and are suitable for different LED lighting cases in the arrays; 3) electro-optical-thermal modeling The combination of optical-electrical-thermal modeling can be used to predict the photothermal parameters of LED arrays with an accuracy of 95 %. The model is very effective in quickly predicting the junction temperature and luminous flux of large LED systems with array structures.

CRediT authorship contribution statement

Minne Liu: Data curation, Formal analysis, Investigation, Visualization, Writing – original draft. **Wenyu Li:** Data curation, Formal

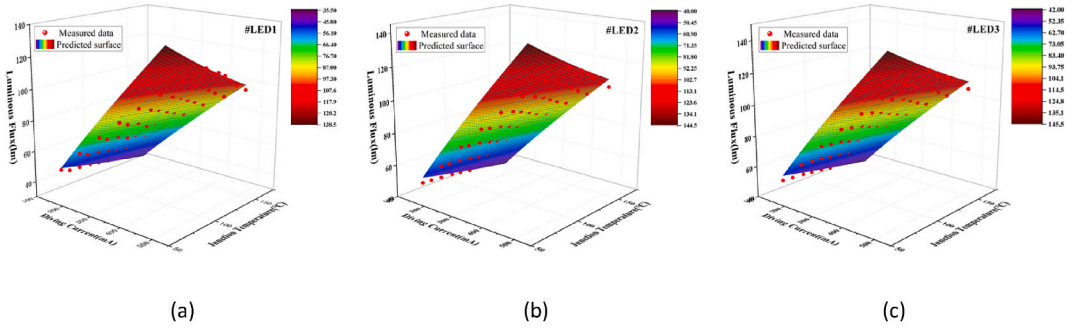

Fig. 15. Fitting results for single LED Model I (a)#LED1; (b)#LED2; (c)#LED3.

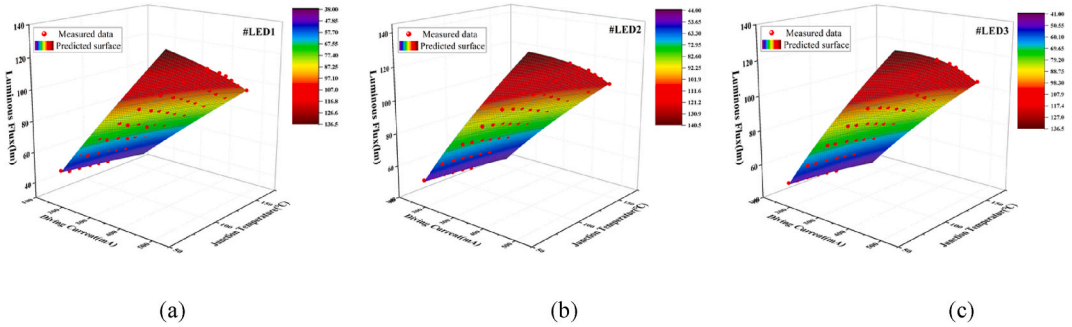

Fig. 16. Fitting results for single LED Model II (a)#LED1; (b)#LED2; (c)#LED3.

Table 6
Model I fitting results.

Sample	D	HC_0	R^2
#LED1	0.86312	0.77636	0.99684
#LED2	0.82419	0.81788	0.99388
#LED3	0.84843	0.81076	0.99263

Table 7
Model II fitting results.

Sample	D	C_e	n	m	HC_0	R^2
#LED1	0.86361	−0.02096	0.97948	1.59403	0.901584	0.99906
#LED2	0.80845	−0.0286	0.95215	1.60895	0.901584	0.99919
#LED3	0.82552	−0.04099	0.91987	1.25231	0.901584	0.99935

Table 8
Luminous flux model results (sample 1 at 0.2A driving current and 40 °C case temperature).

Model (lm)	LED1#	LED2#	LED4#	LED5#	LED array (Experimental:161.45)	Deviation (%)
Model I	49.0557	49.0564	49.0494	49.0494	196.2103	21.53 %
Model II	40.7613	40.7695	40.7695	40.6703	162.8797	8.85 %

analysis, Investigation, Writing – original draft. **Wei Chen:** Investigation, Writing – review & editing. **Mesfin S. Ibrahim:** Investigation, Writing – review & editing. **Jingkang Xiong:** Funding acquisition, Resources. **Guoqi Zhang:** Supervision. **Jiajie Fan:** Conceptualization, Funding acquisition, Project administration, Resources, Supervision, Validation.

Declaration of competing interest

The authors declare that they have no known competing financial interests or personal relationships that could have appeared to influence the work reported in this paper.

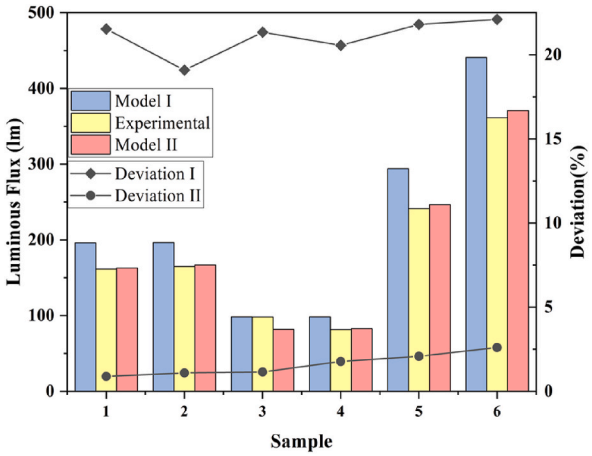

Fig. 17. Comparison of sample luminous flux with experimental results.

Data availability

Data will be made available on request.

Acknowledgment

The work described in this paper was partially supported by the National Natural Science Foundation of China (52275559, 51805147), State Key Laboratory of Applied Optics (SKLAO2022001A01), Shanghai Science and Technology Development Foundation (21DZ2205200), and Changzhou Sci & Tech Program (CZ20230005).

References

[1] N. Holonyak, S.F. Bevacqua, C.V. Bielan, S.J. Lubowski, THE ''DIRECT-INDIRECT'' TRANSITION IN Ga(As1xPx) p-n JUNCTIONS, Appl. Phys. Lett. 3 (3) (1963) 47–49.
[2] G. Grampp, S. Landgraf, Book review: the blue laser diode. By Shuji nakamura, stephen pearton, and gerhard fasol, Adv. Mater. 14 (2) (2002) 170, 170.
[3] S. Liu, X. Luo, LED Packaging for Lighting Applications, Wiley & Sons, 2011, pp. 1–32, https://doi.org/10.1002/9780470827857.
[4] J. Huang, P. Su, J. Ma, Y. Cui, Design method of freeform light distribution lens for LED automotive headlamp based on DMD, in: International Conference on Optical Instruments and Technology 2017, Optical Systems and Modern Optoelectronic Instruments, 2018.
[5] I. Fryc, D. Czyżewski, J. Fan, C.D. Gălăţanu, The drive towards optimization of road lighting energy consumption based on mesopic vision—a suburban street case study, Energies 14 (4) (2021) 1175 [Online], https://www.mdpi.com/1996-1073/14/4/1175.
[6] D. Czyżewski, I. Fryc, The influence of luminaire photometric intensity curve measurements quality on road lighting design parameters, Energies 13 (13) (2020) 3301 [Online], https://www.mdpi.com/1996-1073/13/13/3301.
[7] K.H. Bachanek, B. Tundys, T. Wiśniewski, E. Puzio, A. Marousková, Intelligent street lighting in a smart city concepts—a direction to energy saving in cities: an overview and case study, Energies 14 (11) (2021) 3018 [Online], https://www.mdpi.com/1996-1073/14/11/3018.
[8] S. Fotios, A. Bohm, Road lighting and accidents: cyclists, lighting, accidents and responsibility, Light. J. 82 (5) (2017) 28–32.
[9] J. Li, F. Lin, D. Wang, W. Tian, A loop-heat-pipe heat sink with parallel condensers for high-power integrated LED chips, Appl. Therm. Eng. 56 (1–2) (2013) 18–26.
[10] X.Y. Lu, T.C. Hua, M.J. Liu, Y.X. Cheng, Thermal analysis of loop heat pipe used for high-power LED, Thermochim. Acta 493 (1) (2009) 25–29.
[11] K. Baran, A. Różowicz, H. Wachta, S. Różowicz, D. Mazur, Thermal analysis of the factors influencing junction temperature of LED panel sources, Energies 12 (20) (2019) 3941 [Online], https://www.mdpi.com/1996-1073/12/20/3941.
[12] Xiangbing, et al., Optical Design of LED-Based Automotive Headlamps, Optics & Laser Technology, 2013.
[13] Wei, et al., Reliability assessment of light-emitting diode packages with both luminous flux response surface model and spectral power distribution method, IEEE Access 7 (2019) 68495–68502.
[14] S. Liu, X. Luo, LED Packaging for Lighting Applications: Design, Manufacturing, and Testing, 2011, pp. 317–330, https://doi.org/10.1002/9780470827857.
[15] T. Cheng, X. Luo, S. Huang, L. Sheng, Thermal analysis and optimization of multiple LED packaging based on a general analytical solution, Electron. Compon. Technol. Conf. 49 (1) (2010) 196–201.
[16] S. H. Min, "Thermal Analysis of High Power Led Arrays."..
[17] S.L. Chuang, A. Ishibashi, Kinetic model for degradation of light-emitting diodes, IEEE J. Quant. Electron. 33 (6) (1997) 970–979.
[18] J. Fan, K.C. Yung, M. Pecht, Lifetime estimation of high-power white LED using degradation-data-driven method, IEEE Trans. Device Mater. Reliab. 12 (2) (2012) 470–477.
[19] J. Fan, K.C. Yung, M. Pecht, Physics-of-Failure-Based prognostics and health management for high-power white light-emitting diode lighting, IEEE Trans. Device Mater. Reliab. 11 (3) (2011) 407–416.
[20] J. Xie, M. Pecht, Reliability prediction modeling of semiconductor light emitting device, Electronics Quality 3 (4) (2009) 218–222.
[21] M. Chang, C. Chen, D. Das, M. Pecht, Anomaly detection of light-emitting diodes using the similarity-based metric test, IEEE Trans. Ind. Inf. 10 (3) (2014) 1852–1863.
[22] Z. Lu, BinHenzen PengfeiHuang, ReinderLiao AlexCoehoorn, Guofu HuaZhou, Experimental investigation on the thermal performance of three-dimensional vapor chamber for LED automotive headlamps, Appl. Therm. Eng.: Design, processes, equipment, economics 157 (2019).
[23] K.R. Shailesh, C.P. Kurian, S.G. Kini, Measurement of junction temperature of light-emitting diodes in a luminaire, Light. Res. Technol. 47 (5) (AUG 2015) 620–632, https://doi.org/10.1177/1477153514548696 (in English).
[24] E. Ozuturk, A new method to measure the junction temperature of LEDs, OPTOELECTRONICS AND ADVANCED MATERIALS-RAPID COMMUNICATIONS 13 (1–2) (JAN-FEB 2019) 73–77 (in English).

[25] X. Luo, Z. Mao, J. Yang, S. Liu, Engineering method for predicting junction temperatures of high-power light-emitting diodes, IET Optoelectron. 6 (5) (2012) 230–236.
[26] T. Tamura, T. Setomoto, T. Taguchi, Illumination characteristics of lighting array using 10 candela-class white LEDs under AC 100V operation, J. Lumin. 87 (2000) 1180–1182, https://doi.org/10.1016/S0022-2313(99)00588-8, 05/01.
[27] K. Chen, N. Narendran, Estimating the average junction temperature of AlGaInP LED arrays by spectral analysis, Microelectron. Reliab. 53 (5) (2013) 701–705.
[28] Y. Lin, Study of temperature sensitive optical parameters and junction temperature determination of light-emitting diodes, Appl. Phys. Lett. 100 (20) (2012) 677.
[29] D. Liu, H. Yang, P. Yang, Experimental and numerical approach on junction temperature of high-power LED, Microelectron. Reliab. 54 (5) (2014) 926–931, https://doi.org/10.1016/j.microrel.2014.01.016, 2014/05/01/.
[30] D. Shi, S. Feng, Y. Zhang, Y. Qiao, B. Deng, Thermal investigation of LED array with multiple packages based on the superposition method, Microelectron. J. 46 (7) (2015) 632–636.
[31] H.L. Lu, et al., Efficient measurement of thermal coupling effects on multichip light-emitting diodes, IEEE Trans. Power Electron. 32 (12) (2017) 9280–9292.
[32] J. Fan, W. Chen, W. Yuan, X. Fan, G. Zhang, Dynamic prediction of optical and chromatic performances for a light-emitting diode array based on a thermal-electrical-spectral model, Opt Express 9 (2020).
[33] Y.B. Xiao, Y.F. Zhao, Y.Q. Yang, S. Gao, S. Han, P. Yang, Effects of multi-factors on the junction temperature of LED automotive lamp chips, Microelectron. Reliab. 136 (SEP 2022) 114658, https://doi.org/10.1016/j.microrel.2022.114658.
[34] H. Chen, D. Lin, S. Tan, S.S. Hui, Chromatic, Photometric and Thermal Modeling of LED Systems with Nonidentical LED Devices, IEEE TRANSACTIONS ON POWER ELECTRONICS PE, 2014.
[35] H.Y. Tang, H.Y. Ye, X.P. Chen, C. Qian, G.Q. Zhang, Numerical thermal analysis and optimization of multi-chip LED module using response surface methodology and genetic algorithm, IEEE Access 5 (5) (2017) 16459–16468.
[36] L. Pohl, G. Hantos, J. Hegedüs, M. Németh, Z. Kohári, A. Poppe, Mixed detailed and compact multi-domain modeling to describe CoB LEDs, Energies 13 (2020).
[37] L. Pohl, M. Németh, J. Hegedus, G. Hantos, Z. Kohari, A. Poppe, Multi-Domain Modelling and Simulation of White CoB LEDs, 2019, pp. 1–7.
[38] S. Hui, Y.X. Qin, A general photo-electro-thermal theory for light emitting diode (LED) systems, IEEE Trans. Power Electron. 24 (8) (2009) 1967–1976.
[39] S.Y.R. Hui, An extended photoelectrothermal theory for LED systems: a tutorial from device characteristic to system design for general lighting, IEEE Trans. Power Electron. 27 (11) (2012) 4571–4583.
[40] B.J. Huang, C.W. Tang, Thermal–electrical–luminous model of multi-chip polychromatic LED luminaire, Appl. Therm. Eng. 29 (16) (2009) 3366–3373.
[41] J. Park, C.C. Lee, An electrical model with junction temperature for light-emitting diodes and the impact on conversion efficiency, IEEE Electron. Device Lett. 26 (5) (2005) 308–310.
[42] H.T. Chen, X.H. Tao, S.S.Y. Ron Hui, Estimation of optical power and heat-dissipation coefficient for the photo-electro-thermal theory for LED systems, IEEE Trans. Power Electron. 27 (4) (2012) 2176–2183.
[43] C. Yu, J. Fan, C. Qian, X. Fan, G. Zhang, Luminous flux modeling for high power LED automotive headlamp module, in: 2017 18th International Conference on Electronic Packaging Technology (ICEPT), 2017, pp. 1389–1395, https://doi.org/10.1109/ICEPT.2017.8046695, 16-19 Aug. 2017.